1 **7913 Revision 1**

2 # High-Pressure Experimental Study of

3 # Tetragonal $CaSiO_3$-Pervoskite to 200 GPa

4

5 Ningyu Sun[1,2], Hui Bian[1], Youyue Zhang[1], Jung-Fu Lin[3], Vitali B. Prakapenka[4], Zhu
6 Mao[1,2,*]

7

8 [1]Laboratory of Seismology and Physics of Earth's Interior, School of Earth and
9 Planetary Sciences, University of Science and Technology of China, Hefei, Anhui
10 230026, China

11 [2]CAS Center for Excellence in Comparative Planetology, University of Science and
12 Technology of China, Hefei, Anhui 230026, China

13 [3]Department of Geological Sciences, Jackson School of Geosciences, The University
14 of Texas at Austin, Austin, TX 78712, USA

15 [4]Center for Advanced Radiation Sources, University of Chicago, Chicago, IL 60637,
16 USA

17

Corresponding author: zhumao@ustc.edu.cn

Abstract

In this study, we have investigated the crystal structure and equation of state of tetragonal $CaSiO_3$-perovskite up to 200 GPa using synchrotron X-ray diffraction in laser-heated diamond anvil cells. X-ray diffraction patterns of the quenched $CaSiO_3$-pervoskite above 148 GPa clearly show that 200, 211 and 220 peaks of the cubic phase split into 004+220, 204+312 and 224+400 peak pairs, respectively, in the tetragonal structure, and their calculated full width at half maximum (FWHM) exhibits a substaintial increase with pressure. The distribution of diffraction peaks suggests that the tetragonal $CaSiO_3$-perovskite most likely has an *I*4/*mcm* space group at 300 K between 148 and 199 GPa, while other possibilities might still exist. Using the Birch-Murnaghan equations, we have determined the equation of state of tetragonal $CaSiO_3$-perovskite, yielding the bulk modulus K_{0T}= 227 (21) GPa with the pressure derivative of the bulk modulus, K_{0T}'=4.0 (3). Modeled sound velocities at 580 K and around 50 GPa using our study and literature values show the difference in the compressional (V_P) and shear-wave velocity (V_S) between the tetragonal and cubic phases to be 5.3% and 6.7% respectively. At ~110 GPa and 1000 K, this phase transition will lead to a 4.3% and 9.1% jump in V_P and V_S. Since addition of Ti can elevate the transition temperature, the phase transition from the tetragonal to cubic phase may have a seismic signature compatible with the observed mid-lower mantle discontinuity around the cold subduction slabs which needs to be explored by future studies.

Key words: tetragonal $CaSiO_3$-perovskite, equation of state, structure, high pressure

42

43

44 Introduction

45 $CaSiO_3$-perovskite is one of the most abundant silicate phases and the dominant host
46 of Ca in the Earth's lower mantle (Anderson, 1989; Kesson et al., 1998; Murakami et
47 al., 2005; Ringwood, 1975). In the lower mantle, the volume percentage of
48 $CaSiO_3$-perovskite is estimated to be 5-8 wt.% but could be up to 22-29 wt.% in the
49 subducting mid-ocean ridge basalts (MORBs) (e.g. Anderson, 1989; Harte, 2010;
50 Hirose et al., 2005; Wood, 2000). Recent high-pressure studies have found that
51 shear-wave velocity of $CaSiO_3$-perovskite is substantially lower than the global
52 seismic model PREM (Dziewonski and Anderson, 1981; Greaux et al., 2019; Kawai
53 and Tsuchiya, 2014; Thomson et al., 2019). Enrichment of the recycled MORBs with
54 the low-velocity $CaSiO_3$-perovskite could cause a seismic signature compatible with
55 the large-low shear velocity provinces (Thomson et al., 2019). Experimental studies
56 on the structure and elastic properties of $CaSiO_3$ at high pressures are thus important
57 to understand the composition and structure of the lower mantle (e.g. Komabayashi et
58 al., 2007; Kurashina et al., 2004; Mao et al., 1989; Noguchi et al., 2013; Shim et al.,
59 2000; Sun et al., 2016; Wang et al., 1996; Wood, 2000; Zhang et al., 2006).

60

61 $CaSiO_3$-perovskite has been reported to crystallize in the cubic structure at the
62 expected pressure-temperature conditions of the lower mantle (e.g. Komabayashi et
63 al., 2007; Noguchi et al., 2013; Shim et al., 2000; Sun et al., 2016). However, it can
64 also accommodate a certain amount of minor elements such as Ti (Hirose and Fei,

2002; Kesson et al., 1998; Kesson et al., 1994; Nestola et al., 2018; Wood, 2000), which can elevate the phase transition temperature at lower-mantle pressures and may enable the tetragonal phase to exist in the cold subducting slabs (Kurashina et al., 2004; Thomson et al., 2019). The cubic to tetragonal phase transition with the presence of Ti which is likely to happen beyond 1000-km depth may explain the observed seismic reflections in the mid-lower mantle (Kudo et al., 2012; Thomson et al., 2019).

In contrast to the cubic phase, the crystal structure and equation of state (EoS) of tetragonal $CaSiO_3$-perovskite were not well constrained. The cubic to tetragonal phase transition was proposed to be caused by a second-order structure distortion, and four space groups, including *P*4/*mmm*, *P*4/*mbm*, *I*4/*mmm* and *I*4/*mcm* were proposed for the tetragonal phase (Shim et al., 2002; Stixrude et al., 2007). The occurrence of three potential structures (*P*4/*mbm* and *I*4/*mcm*) can be explained by the octahedral rotations, whereas the *P*4/*mmm* structure could be formed by elongating the *c*-axis of the cubic phase (Shim et al., 2002; Stixrude et al., 2007). Slightly shifting the oxygen atoms position of the cubic phase can change the structure to tetragonal *I*4/*mmm*. In early experimental studies, the *P*4/*mmm* model was applied to analyze the lattice parameters and unit cell volume of tetragonal $CaSiO_3$, yielding a modified *c*/*a* ratio (Z=1) of 0.992-0.998 at 0-100 GPa (Ono et al., 2004; Shim et al., 2002). However, theoretical studies pointed out that the phase transition was second order in nature and should be caused by octahedral rotations (Stixrude et al., 1996; Stixrude et al., 2007). *I*4/*mcm* with the lowest calculated energy is theoretically supported to be the stable structure for the tetragonal $CaSiO_3$ (Stixrude et al., 2007). In contrast to *P*4/*mmm*, *I*4/*mcm* has a modified *c*/*a* ratio increasing from 1.004 at 20 GPa to 1.023 at ~220

GPa (Jung and Oganov, 2005; Stixrude et al., 2007). *I*4/*mcm* was also preferred in a recent experimental study based on the Rietveld refinement results, which give better fits for the peak positions and intensities than other proposed space groups (Chen et al., 2018). Meanwhile, a few theoretical studies using first-principle calculations also suggested an orthorhombic structure for $CaSiO_3$ at high pressures and low temperatures (Akber-Knutson et al., 2002; Li et al., 2006; Magyari-Kope et al., 2002). In addition, the bulk modulus of tetragonal $CaSiO_3$-perovskite is highly uncertain, ranging from 223(6) GPa to 248(8) GPa with a fixed pressure derivative of the bulk modulus at 4 (Chen et al., 2018; Greaux et al., 2019; Ono et al., 2004; Shim et al., 2002; Thomson et al., 2019). The structure and EoS of tetragonal $CaSiO_3$-perovskite at high pressures thus require further investigation.

In this study, we have investigated the structure of $CaSiO_3$-perovskite using synchrotron X-ray diffraction in laser-heated diamond anvil cells (DACs). Our study has significantly extended the experimental pressure to 200 GPa. High-resolution XRD data allow us to provide direct constraints on the crystal structure, lattice parameters, and EoS of the tetragonal phase. These results placed a comprehensive understanding on the structure and EoS of tetragonal $CaSiO_3$-perovskite at high pressures.

Experiments

The starting material was $CaSiO_3$ wollastonite, purchased from Sigma-Aldrich Co. LLC, with purity of 99%. The polycrystalline starting material was ground into fine

113 powder and mixed with 5 wt.% Pt as the pressure standard and laser absorber (Fei et
114 al., 2007). The sample mixture was compressed by a DAC into ~10 μm thick pellets.
115 We further cut the sample foil into small pieces. A small sample piece was
116 sandwiched between two NaCl layers, which were pre-loaded to each side of the DAC.
117 NaCl used as the pressure medium and thermal insulator was pre-dried for more than
118 5 hours at ~105℃ to avoid any potential contamination of water in the air. The sample
119 sandwiches were loaded into symmetric DACs with 75/300 μm beveled diamonds
120 anvils. The high-pressure and -temperature XRD experiments were performed at the
121 GeoSoilEnviroConsortium (GSECARS) of the Advanced Photon Source (APS),
122 Argonne National Laboratory (ANL), with an X-ray wavelength of 0.3344 Å.
123 Previous studies have shown that cubic $CaSiO_3$-perovskite is stable up to 156 GPa
124 and will transform into tetragonal phase after quench (e.g. Noguchi et al., 2013; Shim
125 et al., 2000; Sun et al., 2016). Here we directly compressed the cell to ~160 GPa at
126 300 K and then performed laser heating. The diffraction patterns were collected at
127 every 10-15 GPa from 1400 K to 2600 K up to 203 GPa. Assuming Graybody
128 radiation, the temperature was determined by fitting the thermal radiation spectrum
129 using the Planck radiation function (Prakapenka et al., 2008). Diffraction patterns
130 were also collected at 300 K after each heating cycle at high pressures.

131

132 Result

133 The starting $CaSiO_3$ wollastonite became amorphous at 160 GPa and 300 K. Heating
134 the amorphous material immediately transformed $CaSiO_3$ to the cubic perovskite
135 structure (Fig. 1). Continuing heating cubic $CaSiO_3$-perovskite up to 2600 K did not
136 cause any notable change in the XRD patterns. Yet the quenched sample at 300 K and

148 GPa has exhibited an obvious splitting of XRD peaks at 12.0°, 14.7°, and 16.9° (wavelength = 0.3344 Å), respectively. In particular, we observed a new peak at ~10.0-10.2° in the diffraction patterns after quench. The occurrence of the peak is consistent with the *I*4/*mcm* structure which was not reported or not clearly identified in previous experimental studies (Fig. 2) (Chen et al., 2018; Ono et al., 2004; Shim et al., 2002; Thomson et al., 2019). Further analysis of the obtained XRD patterns revealed that $CaSiO_3$ was stable in the cubic perovskite structure between 158 and 203 GPa at 1400-2600 K, but transformed to the tetragonal phase after quench. Calculated deviatoric stress at 300 K using collected diffraction patterns of Pt is less than 1.2 GPa at pressures up to 199 GPa (Fig. 1).

Here we focused on the lattice parameters and EoS of tetragonal $CaSiO_3$-perovskite (Fig. 3). Experimental data of Sun et al. (2016) between 24 and 124 GPa at 300 K have been re-analyzed to better constrain the lattice parameters and pressure-volume relationship of the tetragonal phase at an extended pressure range. For *I*4/*mcm*, *c*-axis is longer than *a*-axis (Table 1). The pressure-volume data were fitted using the Birch-Murnaghan EoS (Birch, 1938) (Fig. 3 and Table 2):

$$P = \frac{3}{2} K_{0T} \left[\left(\frac{V}{V_0} \right)^{-7/3} - \left(\frac{V}{V_0} \right)^{-5/3} \right] \cdot \left\{ 1 + \frac{3}{4} \left(K' - 4 \right) \left[\left(\frac{V}{V_0} \right)^{-2/3} - 1 \right] \right\},$$

where K_{0T} and V_0 are the isothermal bulk modulus and unit cell volume at the ambient conditions, respectively. *K*' is the pressure derivative of the bulk modulus. To have a better comparison with previous experimental and theoretical results, we normalized the *Z* number of the tetragonal phase to 1. In the normalized unit cell, *c* equals that of the tetragonal $CaSiO_3$-perovskite with *Z*=4 divided by 2, while *a* equals the initial *a*

160 divided by $\sqrt{2}$ (Chen et al., 2018; Jung and Oganov, 2005; Ono et al., 2004; Shim et
161 al., 2002). Here, with a free fitting of *K*', we obtained the modified V_0 = 45.6(4) Å^3
162 (Z=1), K_{0T} = 227(21) GPa and *K*'=4.0 (3).

163

164 ## Discussion

165 Due to the similarity in the XRD patterns between the cubic and tetragonal $CaSiO_3$,
166 the stable structure of $CaSiO_3$ at high pressure-temperature conditions has been under
167 debate for years (Chen et al., 2018; Jung and Oganov, 2005; Ono et al., 2004; Shim et
168 al., 2002; Stixrude et al., 2007). Splitting of the cubic 200 peak was applied to
169 determine the occurrence of the phase transition at high pressures (Chen et al., 2018;
170 Komabayashi et al., 2007; Kurashina et al., 2004; Noguchi et al., 2013; Ono et al.,
171 2004; Shim et al., 2002; Sun et al., 2016). Here, our obtained XRD patterns above 148
172 GPa showed a well-resolved splitting of the cubic 200, 211 and 220 peaks after
173 quench, while previous studies were not as clear or only observed several of them
174 (Chen et al., 2018; Ono et al., 2004; Shim et al., 2002). Using the space groups and
175 lattice parameters, we also calculated the full width at half maximum (FWHM) of the
176 tetragonal 004+220, 204+312, and 224+400 peak pairs at high pressure and 300 K
177 (Fig. 4). Across the cubic-tetragonal transition, the 200, 211, and 220 peaks of the
178 cubic phase split into 004+220, 204+312, and 224+400 peaks, respectively, in the
179 tetragonal phase. The FWHM of the peak pairs in the tetragonal structure exhibit a
180 substantial increase with pressure up to 200 GPa. It is thus easier to identify the
181 presence of tetragonal $CaSiO_3$-perovskite from the XRD patterns at pressures above
182 148 GPa, but also make the fitting of volume and lattice parameter more accurate.
183 Previous studies mentioned that the observed peak splitting may be a result of the

increased deviatoric stress inside the DAC, and a deviatoric stress of ~7 GPa is enough to induce the peak splitting at temperatures as high as 1550 K (Chen et al., 2018; Shim et al., 2002). Here we showed that the diffraction patterns after quench have a deviatoric stress less than 1.2 GPa up to 199 GPa (Singh, 1993; Sun et al., 2016) (Fig. 1). The peak splitting in the quenched sample can only be caused by the phase transition but not by the deviatoric stress (Chen et al., 2018; Shim et al., 2002).

More importantly, we have observed the presence of an additional peak with 2θ at ~10.0-10.2^o from 148 to 199 GPa at 300 K (d-spacing of 1.92-1.88 Å) (Fig. 2). Among four potential structures, this peak with 2θ at ~10.0-10.2^o assigned as peak 211 in the tetragonal structure only be explained by $I4/mcm$, but was not observed in previous experimental work (Chen et al., 2018; Ono et al., 2004; Shim et al., 2002). Although Sun et al. (2016) did observe the 211 peak, their motivation is to determine the thermal EoS of cubic $CaSiO_3$-perovskite. We also examined the XRD patterns of tetragonal $CaSiO_3$-perovskite in Sun et al. (2016) between 24 and 124 GPa at 300 K which also recorded the tetragonal 211 peak as a continuous ring (Fig. 2). Rotation of the sample when collecting the XRD patterns help us to reveal the 211 peak more clearly as a relatively continuous ring in the cake patterns (Fig. 2) (Ma et al., 2004; Smith and Desgreniers, 2009). The presence of peak 211 is a new indicator for the cubic to tetragonal phase transition and provides an additional constraint on the lattice parameter a and c. With obtained XRD patterns, a-axis of the tetragonal $I4/mcm$ phase is calculated to be ~2.5% shorter than that of the cubic phase because of the distortion in structure. With Z=1, previous experimental studies reported a modified c/a value less than 1 for the $P4/mmm$ phase (Fig. 5) (Chen et al., 2018; Jung and Oganov, 2005; Ono et al., 2004; Shim et al., 2002; Stixrude et al., 2007). For the $I4/mcm$ structure,

c-axis is longer than *a*-axis, leading to a modified *c*/*a* ratio greater than 1. The modified *c*/*a* ratio of the tetragonal $CaSiO_3$-perovskite increases from ~1.003 at 24 GPa to ~1.012 at 199 GPa (Fig. 5). The modified *c*/*a* ratio showing here between 24 and 199 GPa is in general agreement with a recent experimental study and follows a similar trend with pressure as the theoretical predictions (Chen et al., 2018; Stixrude et al., 2007).

The unit cell volume of the *I*4/*mcm* phase at a given pressure shown here is slightly smaller than that reported in previous studies using the *P*4/*mmm* structure (Ono et al., 2004; Shim et al., 2002). The difference is caused by using different sequence of peaks in two space groups to analyze the XRD pattern. If the *P*4/*mmm* structure is used to calculate unit-cell volume of the tetragonal $CaSiO_3$ by neglecting the 211 peak, the calculated volume is similar to that shown in previous studies (Fig. 3) (Ono et al., 2004; Shim et al., 2002). Above 45 GPa, the unit cell volume of the *P*4/*mmm* structure in Ono et al., (2004) are greater than other results, potentially due to large deviatoric stress with no pressure medium in the high-pressure experiments (Chen et al., 2018; Shim et al., 2002; Thomson et al., 2019). K_{0T} of the tetragonal $CaSiO_3$-perovskite with a fixed K_{0T}'=4 is highly uncertain, ranging from 223(6) GPa to 248(8) GPa in previous experimental studies (Chen et al., 2018; Greaux et al., 2019; Ono et al., 2004; Shim et al., 2002; Thomson et al., 2019). Here, fitting the *P*-*V* data at a much larger pressure range up to 200 GPa yielded K_{0T} of 227(21) with a free *K*'. For a better comparison, we re-analyzed the previous experimental *P*-*V* data using a self-consistent pressure scale of Fei et al., (2007) for a better comparison (Table 2) (Shim et al., 2002; Ono et al., 2004; Chen et al., 2018; Thomson et al., 2019; Jung and Oganov, 2005; Stixrude et al., 2007; Caracas et al., 2005). Previous experimental

studies with a much lower K_{0T} could be caused by limited experimental pressure range at 300 K or the untransformed lower-pressure materials (Chen et al., 2018; Ono et al., et al., 2004; Thomson et al., 2019; Gréaux et al., 2019). K_{0T} of the tetragonal phase in Shim et al. (2002) is much greater than our and other literature results, potentially due to their limited experimental data points and narrow pressure range (Chen et al., 2018; Ono et al., et al., 2004). In addition, tetragonal $CaSiO_3$-perovskite has a slightly lower K_{0T} than the cubic phase, although a few experimental studies reported a low K_{0T} of 208-237 GPa for the cubic phase (Greaux et al., 2019; Kawai and Tsuchiya, 2014; Noguchi et al., 2013; Ricolleau et al., 2009; Shim et al., 2000; Shim et al., 2002; Wang et al., 1996; Zhang et al., 2006).

Geophysical implications

A recent experimental study showed that addition of Ti in $CaSiO_3$-perovskite could elevate the phase transition temperature from the cubic to the tetragonal phase (Thomson et al., 2019). Ti-bearing tetragonal $CaSiO_3$-perovskite may exist in the cold subducting slabs in the Earth's lower mantle (Ono et al., 2004; Thomson et al., 2019). Here we modeled the sound velocity of tetragonal and cubic endmember $CaSiO_3$-perovskite using our obtained EoS together with literature results (Fig. 6) (Gréaux et al., 2019; Thomson et al., 2019). Because of the second order transition, the density of the tetragonal $CaSiO_3$-perovskite along the phase boundary will be the same as the cubic phase. The phase boundary between the tetragonal and cubic $CaSiO_3$-perovskite was only determined at ~50 GPa and 580 K by Kurashina et al. (2004). Here we modeled the velocity change across the phase transition at 580 K between 40 and 60 GPa. Using the estimated Clapeyron slope in Kurashina et al.

(2004), the tetragonal to cubic phase transition temperature is estimated to be ~1000 K between 100 and 120 GPa. The velocity change across the phase transition between 100 and 120 GPa was also shown in Fig. 6. For the cubic phase, Thomson et al. (2019) and Gréaux et al. (2019) reported different bulk and shear moduli as well as their pressure and temperature derivatives. Both of their results were used to calculate the sound velocities of the cubic phase. The obtained K_{0T}, K' and V_0 in this study together with necessary parameters in Thomson et al. (2019) and Gréaux et al. (2019) were used to calculated the velocity of the tetragonal phase. Due to lack experimental constraints, some thermoelastic parameters of tetragonal $CaSiO_3$-perovskite, such as dK/dT and dG/dT, were assumed to be the same as the cubic phase (Thomson et al., 2019; Gréaux et al., 2019). Uncertainties of the calculated sound velocities because of using different literature elastic parameters were shown in shading in Fig. 6 (Gréaux et al., 2019; Thomson et al., 2019).

The compressional (V_P) and shear-wave velocities (V_S) of tetragonal $CaSiO_3$-perovskite are ~5.3% and ~6.7% lower than the cubic phase at ~50 GPa and 580 K, respectively (Fig. 6). At 1000 K and 100 GPa, the difference in V_P and V_S between the cubic and tetragonal phase is ~4.3% and ~9.1 %, respectively. In the subducted oceanic crust, the volume percentage of $CaSiO_3$-perovskite could be as great as 22-29% (e.g. Anderson, 1989; Harte, 2010; Hirose et al., 2005; Wood, 2000). The velocity jump caused by the tetragonal to cubic phase transition in $CaSiO_3$-perovskite will be 1.3% in V_P and 1.7% in V_S at ~50 GPa, and 1.1% in V_P and 2.3% in V_S at ~110 GPa in the cold subduction oceanic crust. Without experimental constraints on the influence of Ti on the phase boundary and thermal elastic properties of the tetragonal and cubic phases, our modeling can only provide a preliminary

283 estimation on the influence of the phase transition of $CaSiO_3$ on the velocity profiles
284 of the lower mantle.

285

286 In summary, the structure of $CaSiO_3$ has been studied up to 200 GPa by synchrotron
287 XRD in laser-heated DACs. Quenching to 300 K leads to the transition of $CaSiO_3$
288 from the cubic to tetragonal structure. Compared to previous experimental results,
289 here we have observed more distinct splitting of the cubic 200, 211, and 220 peaks
290 after temperature quench between 148 and 199 GPa. The new peak 211 with 2θ
291 around 10.0-10.2^o was consistent with the *I*4/*mcm* structure. We note that the *I*4/*mcm*
292 tetragonal phase has a modified *c*/*a* ratio (*Z*=1) greater than 1, which increases from
293 1.002 at ~20 GPa to 1.012 at ~200 GPa. The obtained K_{0T} of the *I*4/*mcm* phase is
294 smaller than that of the cubic $CaSiO_3$-perovskite. The comparison in V_P and V_S
295 between tetragonal and cubic $CaSiO_3$-perovskite at high temperature and pressure is
296 useful to estimate the influence of the phase transition on the velocity profiles of the
297 lower mantle, indicating the phase transition can cause substantial increase in the
298 sound velocity. Future studies are expected to determine the effect of Ti on the
299 thermoelastic parameters of tetragonal $CaSiO_3$-perovskite and provide new insights in
300 understanding the composition and structure of the lower mantle.

301

302 **Acknowledgement**

303 Z. Mao acknowledges supports from the National Science Foundation of China
304 (41874101), Strategic Priority Research Program of the Chinese Academy of Sciences
305 (XDB41000000), National Key R&D Program of China (2018YFA0702703), Funds

for leading talents of USTC (KY2080000061). N. Sun acknowledges supports from Fundamental Research Funds for the Central Universities (WK2080000133). J. F. Lin acknowledges support from Geophysics Program of the National Science Foundation (EAR-1916941). Portions of this work were performed at GeoSoilEnviroCARS (The University of Chicago, Sector 13), Advanced Photon Source (APS), Argonne National Laboratory. GeoSoilEnviroCARS is supported by the National Science Foundation-Earth Sciences (EAR-1634415) and Department of Energy- GeoSciences (DE-FG02-94ER14466). This research used resources of the Advanced Photon Source, a U.S. Department of Energy (DOE) Office of Science User Facility operated for the DOE Office of Science by Argonne National Laboratory under Contract No. DE-AC02-06CH11357.

References

Akber-Knutson, S., Bukowinski, M.S.T., and Matas, J. (2002) On the structure and compressibility of $CaSiO_3$ perovskite. Geophysical Research Letters, 29(3), doi:10.1029/2001GL013523

Anderson, D.L. (1989) Theory of the Earth. Blackwell Scientific Publications, Oxford.

Birch, F. (1938) The effect of pressure upon the elastic parameters of isotropic solids, according to Murnaghan's theory of finite strain. Journal of Applied Physics, 9(4), 279-288.

Caracas, R., Wentzcovitch, R., Price, G.D., and Brodholt, J. (2005) $CaSiO_3$ Perovskite at Lower Mantle Pressures. Geophysical Research Letters, 32(6), doi:

10.1029/2004GL022144.

Chen, H., Shim, S., Leinenweber, K., Prakapenka, V., Meng, Y., and Prescher, C. (2018) Crystal structure of $CaSiO_3$ perovskite at 28-62 GPa and 300 K under Quasi-Hydrostatic stress conditions. American Mineralogist: Journal of Earth and Planetary Materials, 103(3), 462-468.

Dziewonski, A.M., and Anderson, D.L. (1981) Preliminary Reference Earth Model. Physics of the Earth and Planetary Interiors, 25(4), 297-356.

Fei, Y.W., Ricolleau, A., Frank, M., Mibe, K., Shen, G.Y., and Prakapenka, V. (2007) Toward an internally consistent pressure scale. Proceedings of the National Academy of Sciences of the United States of America, 104(22), 9182-9186.

Greaux, S., Irifune, T., Higo, Y., Tange, Y., Arimoto, T., Liu, Z.D., and Yamada, A. (2019) Sound velocity of $CaSiO_3$ perovskite suggests the presence of basaltic crust in the Earth's lower mantle. Nature, 565(7738), 218-221.

Harte, B. (2010) Diamond formation in the deep mantle: the record of mineral inclusions and their distribution in relation to mantle dehydration zones. Mineralogical Magazine, 74(2), 189-215.

Hirose, K., and Fei, Y.W. (2002) Subsolidus and melting phase relations of basaltic composition in the uppermost lower mantle. Geochimica Et Cosmochimica Acta, 66(12), 2099-2108.

Hirose, K., Takafuji, N., Sata, N., and Ohishi, Y. (2005) Phase transition and density of subducted MORB crust in the lower mantle. Earth and Planetary Science Letters, 237(1-2), 239-251.

Jung, D.Y., and Oganov, A.R. (2005) Ab initio study of the high-pressure behavior of $CaSiO_3$ perovskite. Physics and Chemistry of Minerals, 32(2), 146-153.

Kawai, K., and Tsuchiya, T. (2014) P-V-T equation of state of cubic $CaSiO_3$ perovskite from first-principles computation. Journal of Geophysical Research-Solid Earth, 119(4), 2801-2809.

Kesson, S.E., Fitz Gerald, J.D., and Shelley, J.M. (1998) Mineralogy and dynamics of a pyrolite lower mantle. Nature, 393(6682), 252-255.

Kesson, S.E., Fitz Gerald, J.D., and Shelley, J.M.G. (1994) Mineral Chemistry and Density Subducted Basaltic Crust at Lower-Mantle Pressures. Nature, 372(6508), 767-769.

Komabayashi, T., Hirose, K., Sata, N., Ohishi, Y., and Dubrovinsky, L.S. (2007) Phase transition in $CaSiO_3$ perovskite. Earth and Planetary Science Letters, 260(3-4), 564-569.

Kudo, Y., Hirose, K., Murakami, M., Asahara, Y., Ozawa, H., Ohishi, Y., and Hirao, N. (2012) Sound velocity measurements of $CaSiO_3$ perovskite to 133 GPa and implications for lowermost mantle seismic anomalies. Earth and Planetary Science Letters, 349, 1-7.

Kurashina, T., Hirose, K., Ono, S., Sata, N., and Ohishi, Y. (2004) Phase transition in Al-bearing $CaSiO_3$ perovskite: implications for seismic discontinuities in the lower mantle. Physics of the Earth and Planetary Interiors, 145(1-4), 67-74.

Li, L., Weidner, D.J., Brodholt, J., Alfe, D., Price, G.D., Caracas, R., and Wentzcovitch, R. (2006) Phase stability of $CaSiO_3$ perovskite at high pressure and temperature: Insights from ab initio molecular dynamics. Physics of the Earth and Planetary Interiors, 155(3-4), 260-268.

Ma, Y.Z., Somayazulu, M., Shen, G.Y., Mao, H.K., Shu, J.F., and Hemley, R.J. (2004) In situ X-ray diffraction studies of iron to Earth-core conditions. Physics of the Earth and Planetary Interiors, 143, 455-467.

Magyari-Kope, B., Vitos, L., Grimvall, G., Johansson, B., and Kollar, J. (2002) Low-temperature crystal structure of $CaSiO_3$ perovskite: An ab initio total energy study. Physical Review B, 65(19), doi:10.1103/PhysRevB.65.193107.

Mao, H.K., Chen, L.C., Hemley, R.J., Jephcoat, A.P., Wu, Y., and Bassett, W.A. (1989) Stability and Equation of State of $CaSiO_3$-Perovskite to 134 Gpa. Journal of Geophysical Research-Solid Earth and Planets, 94(B12), 17889-17894.

Murakami, M., Hirose, K., Sata, N., and Ohishi, Y. (2005) Post-perovskite phase transition and mineral chemistry in the pyrolitic lowermost mantle. Geophysical Research Letters, 32(3), doi:10.1029/2004GL021956.

Nestola, F., Korolev, N., Kopylova, M., Rotiroti, N., Pearson, D.G., Pamato, M.G., Alvaro, M., Peruzzo, L., Gurney, J.J., Moore, A.E., and Davidson, J. (2018) $CaSiO_3$ perovskite in diamond indicates the recycling of oceanic crust into the lower mantle. Nature, 555(7695), 237-241.

Noguchi, M., Komabayashi, T., Hirose, K., and Ohishi, Y. (2013) High-temperature compression experiments of $CaSiO_3$ perovskite to lowermost mantle conditions and its thermal equation of state. Physics and Chemistry of Minerals, 40(1), 81-91.

Ono, S., Ohishi, Y., and Mibe, K. (2004) Phase transition of Ca-perovskite and stability of Al-bearing Mg-perovskite in the lower mantle. American Mineralogist, 89(10), 1480-1485.

Prakapenka, V.B., Kubo, A., Kuznetsov, A., Laskin, A., Shkurikhin, O., Dera, P., Rivers, M.L., and Sutton, S.R. (2008) Advanced flat top laser heating system for high pressure research at GSECARS: application to the melting behavior of germanium. High Pressure Research, 28(3), 225-235.

Ricolleau, A., Fei, Y.W., Cottrell, E., Watson, H., Deng, L.W., Zhang, L., Fiquet, G., Auzende, A.L., Roskosz, M., Morard, G., and Prakapenka, V. (2009) Density profile of pyrolite under the lower mantle conditions. Geophysical Research Letters, doi:10.1029/2008GL036759.

Ringwood, A.E. (1975) Composition and petrology of the Earth's mantle. xvi, 618 p. p. McGraw-Hill, New York,.

Shim, S.H., Duffy, T.S., and Shen, G.Y. (2000) The stability and P-V-T equation of state of $CaSiO_3$ perovskite in the Earth's lower mantle. Journal of Geophysical Research-Solid Earth, 105(B11), 25955-25968.

Shim, S.H., Jeanloz, R., and Duffy, T.S. (2002) Tetragonal structure of $CaSiO_3$ perovskite above 20 GPa. Geophysical Research Letters, 29(24), doi:10.1029/2002GL016148,.

Smith, J.S., and Desgreniers, S. (2009) Selected techniques in diamond anvil cell crystallography: centring samples using X-ray transmission and rocking powder samples to improve X-ray diffraction image quality. Journal of

Synchrotron Radiation, 16, 83-96.

Stixrude, L., Lithgow-Bertelloni, C., Kiefer, B., and Fumagalli, P. (2007) Phase stability and shear softening in $CaSiO_3$ perovskite at high pressure. Physical Review B, 75(2), doi: 10.1103/PhysRevB.75.024108. .

Sun, N.Y., Mao, Z., Yan, S., Wu, X., Prakapenka, V.B., and Lin, J.F. (2016) Confirming a pyrolitic lower mantle using self-consistent pressure scales and new constraints on $CaSiO_3$ perovskite. Journal of Geophysical Research-Solid Earth, 121(7), 4876-4894.

Thomson, A., Crichton, W., Brodholt, J., Wood, J., Siersch, N., Muir, J., Dobson, D.P., and Hunt, S. (2019) Seismic velocities of $CaSiO_3$ perovskite can explain LLSVPs in Earth's lower mantle. Nature, 572, 643-647.

Wang, Y.B., Weidner, D.J., and Guyot, F. (1996) Thermal equation of state of $CaSiO_3$ perovskite. Journal of Geophysical Research-Solid Earth, 101(B1), 661-672.

Wood, B.J. (2000) Phase transformations and partitioning relations in peridotite under lower mantle conditions. Earth and Planetary Science Letters, 174(3-4), 341-354.

Zhang, Y.G., Zhao, D.P., Matsui, M., and Guo, G.J. (2006) Equations of state of $CaSiO_3$ Perovskite: a molecular dynamics study. Physics and Chemistry of Minerals, 33(2), 126-137.

440 Table 1. Pressure-volume data of tetragonal $CaSiO_3$-perovskite at high pressures and
441 300 K

P (GPa)	a (Å)	c (Å)	V (Å^3)
21.5(4)*	4.904(2)	6.947(3)	167.0(2)
24.9(6)*	4.882(3)	6.926(4)	165.1(3)
30.2(5)*	4.875(2)	6.920(3)	164.4(2)
38.4(7)*	4.837(1)	6.868(3)	160.7(1)
43.6(11)*	4.822(3)	6.823(5)	158.7(3)
52.0(13)*	4.776(2)	6.796(3)	155.0(2)
57.0(15)*	4.753(4)	6.747(5)	152.4(4)
59.9(15)*	4.743(2)	6.741(3)	151.7(2)
63.4(16)*	4.741(2)	6.731(3)	151.3(2)
69.9(17)*	4.717(3)	6.701(4)	149.1(3)
84.4(21)*	4.673(1)	6.651(2)	145.2(1)
93.4(24)*	4.643(2)	6.621(3)	142.7(2)
98.1(26)*	4.621(4)	6.585(5)	140.6(4)
124.0(30)*	4.565(3)	6.503(5)	135.5(3)
148.3(36)	4.502(3)	6.433(5)	130.4(3)
148.4(36)	4.500(3)	6.430(5)	130.2(3)
159.2(38)	4.481(2)	6.400(4)	128.5(2)
163.3(40)	4.471(2)	6.384(3)	127.6(2)
171.4(41)	4.460(2)	6.374(3)	126.8(2)
172.6(41)	4.461(1)	6.378(2)	126.9(1)
179.2(43)	4.449(3)	6.356(2)	125.8(2)
193.1(48)	4.428(3)	6.333(5)	124.2(3)
199.2(47)	4.415(2)	6.315(4)	123.1(2)

*Sun et al. (2016)

442

443 Table 2. EoS of the tetragonal $CaSiO_3$-perovskite under self-consistent pressure scales

	This study	This study	Shim 2002	Ono 2004	Chen 2018	Thomson 2019	Jung 2005*	Stixrude 2007*	Caracas 2005*
K_{0T} (GPa)	227 (21)	229 (4)	259 (5)	235 (9)	228(6)	224(4)	219.04	252	249
K'	4.0 (3)	4#	4#	4#	4#	4#	4.08	4.1	4.09
V_0 (Å^3)	45.6(4)	45.6(2)	45.58f	45.9 (4)	46.2(1)	46.10(6)	46.89	44.00	44.537

444

445 #fixed

446 *theoretical results, under 0 K

447

448 ## Figure caption

449 Figure 1. (a) Experimental pressure-temperature conditions of $CaSiO_3$-perovskite.
450 Blue: cubic $CaSiO_3$-perovskite; red: tetragonal $CaSiO_3$-perovskite; solid circles: this
451 study; open circles: Sun et al. (2016); diamonds: Noguchi et al. (2013); squares:
452 Kurashina et al. (2004); grey lines: typical lower mantle geotherm and a
453 representative cold slab geotherm, respectively (Brown and Shankland, 1981; Kirby et
454 al., 1996); dashed black lines: phase boundary between the cubic and tetragonal
455 phases based on previous experimental results (Kurashina et al., 2004; Noguchi et al.,
456 2013; Sun et al., 2016); (b) Calculated deviatoric stress (absolute value) at 300 K.
457 Solid circles: this study; open circles: calculated using results in Sun et al. (2016).

458

459 Figure 2. XRD patterns of $CaSiO_3$-perovskite at high pressures. (a) Representative
460 XRD patterns of $CaSiO_3$-perovskite at high pressures and temperatures. Red line:
461 cubic $CaSiO_3$-perovskite at 170 GPa and 2500 K; blue line: tetragonal
462 $CaSiO_3$-perovskite at 163 GPa and 300 K; (b) Cake patterns of tetragonal

463 $CaSiO_3$-perovskite at 163 GPa and 44 GPa, respectively. The characteristic 211 peak
464 at 2θ around 10^o in the *I*4/*mcm* tetragonal phase is shown as a continuous ring; X-ray
465 wavelength is 0.3344 Å.

466

467 Figure 3. Pressure-volume relationship of tetragonal $CaSiO_3$-perovskite at high
468 pressures and 300 K. Red circles and line: the *I*4/*mcm* phase in this study; green
469 circles: the *P*4/*mmm* phase (Shim et al., 2002); blue circles: the *P*4/*mmm* phase (Ono
470 et al., 2004); orange circles: the *I*4/*mcm* phase (Chen et al., 2018); grey circles: this
471 study assuming a *P*4/*mmm* tetragonal structure; black lines: calculated volume of the
472 cubic $CaSiO_3$-perovskite at 300 K (Sun et al., 2016).

473

474 Figure 4. Modeled peak widths of the tetragonal phase at high pressures. Orange:
475 tetragonal peak 004+220 from splitting of the cubic 200 peak after quench; red:
476 tetragonal peak 204+312 from splitting of the cubic 211 peak after quench; blue:
477 tetragonal peak 224+400 from splitting of the cubic 220 peak after quench.

478

479 Figure 5. Lattice parameters of tetragonal $CaSiO_3$-perovskite. (a) Variation of *a* and *c*
480 axis of tetragonal $CaSiO_3$-perovskite with pressure at 300 K. Blue: *c*-axis; red: *a*-axis;
481 (b) The modified *c*/*a* ratio of tetragonal $CaSiO_3$-perovskite at high pressures and 300
482 K. Red: this study; green: Shim et al. (2002); blue: Ono et al. (2004); orange: Chen et
483 al. (2018); purple: (Stixrude et al. (2007)).

484

Figure 6. Modeled compressional (V_P) and shear-wave velocities (V_S) of $CaSiO_3$-perovskite at at ~50 GPa and 110 GPa. (a) Calculated velocities at 580 K between 40 and 60 GPa and at 1000 K between 100 and 120 GPa; Solid lines: tetragonal phase; dashed lines: cubic phase; blue: V_S and V_P at 580 K; red: V_S and V_P at 1000 K; bold lines: calculated using results from this work and Gréaux et al. (2019); thin lines: calculated using results from this work and Thomson et al. (2019). (b) The shear-wave velocity change ΔV_S aross the tetragonal to cubic phase transition; (c) The compressional-wave velocity change ΔV_P aross the tetragonal to cubic phase transition. Bold lines: calculated using results from this work and Gréaux et al. (2019); thin line: calculated using results from this work and Thomson et al. (2019). Density was assumed to be the same for both tetragonal and cubic phases due to the second-order phase transition. Vertical ticks represent the calculation errors using standard error propagation from the used parameters.

This is the peer-reviewed, final accepted version for American Mineralogist, published by the Mineralogical Society of America.
The published version is subject to change. Cite as Authors (Year) Title. American Mineralogist, in press.
DOI: https://doi.org/10.2138/am-2021-7913. http://www.minsocam.org/

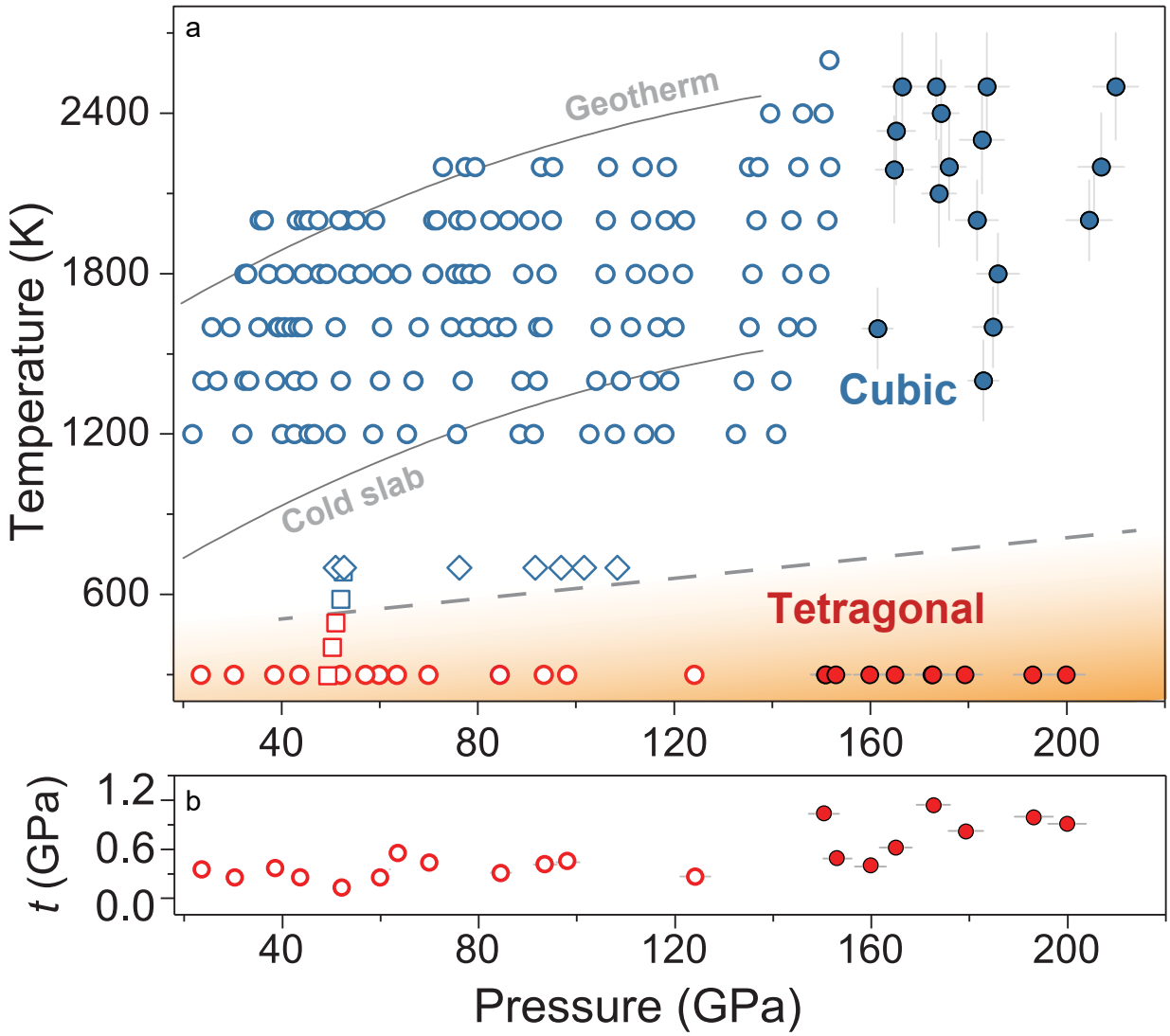

Figure 1

This is the peer-reviewed, final accepted version for American Mineralogist, published by the Mineralogical Society of America.
The published version is subject to change. Cite as Authors (Year) Title. American Mineralogist, in press.
DOI: https://doi.org/10.2138/am-2021-7913. http://www.minsocam.org/

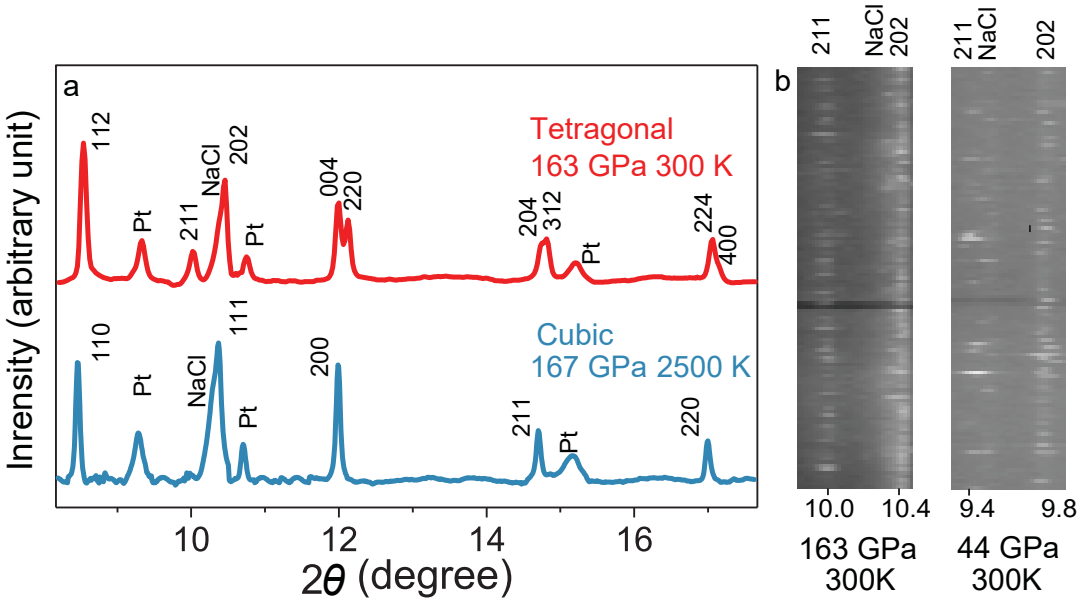

Figure 2

This is the peer-reviewed, final accepted version for American Mineralogist, published by the Mineralogical Society of America.
The published version is subject to change. Cite as Authors (Year) Title. American Mineralogist, in press.
DOI: https://doi.org/10.2138/am-2021-7913. http://www.minsocam.org/

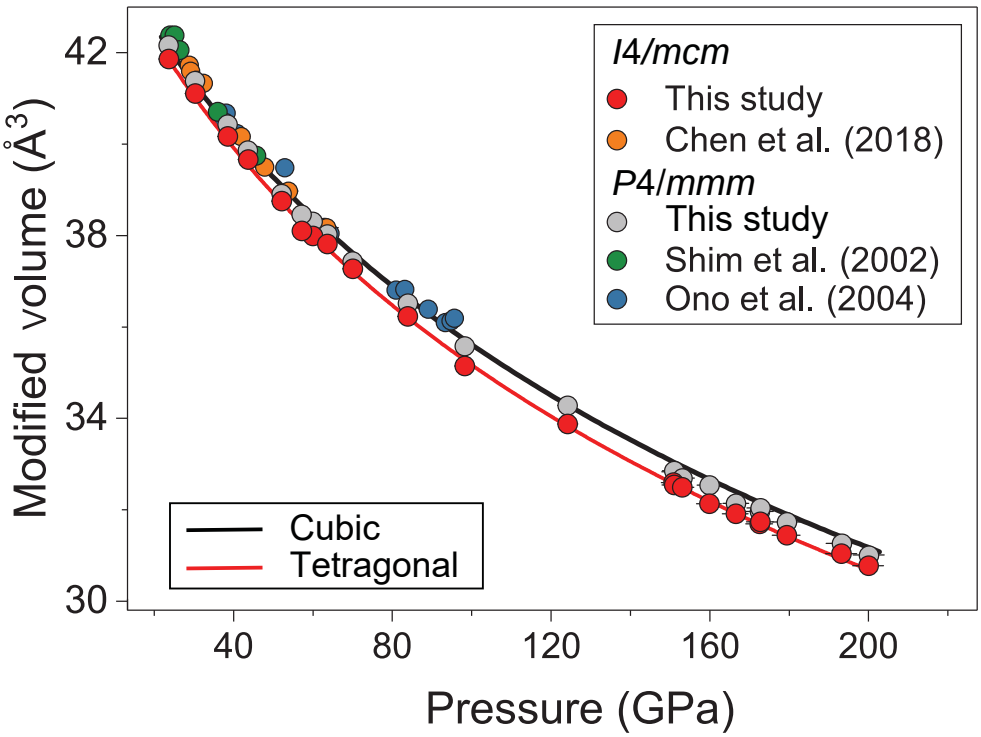

Figure 3

This is the peer-reviewed, final accepted version for American Mineralogist, published by the Mineralogical Society of America.
The published version is subject to change. Cite as Authors (Year) Title. American Mineralogist, in press.
DOI: https://doi.org/10.2138/am-2021-7913. http://www.minsocam.org/

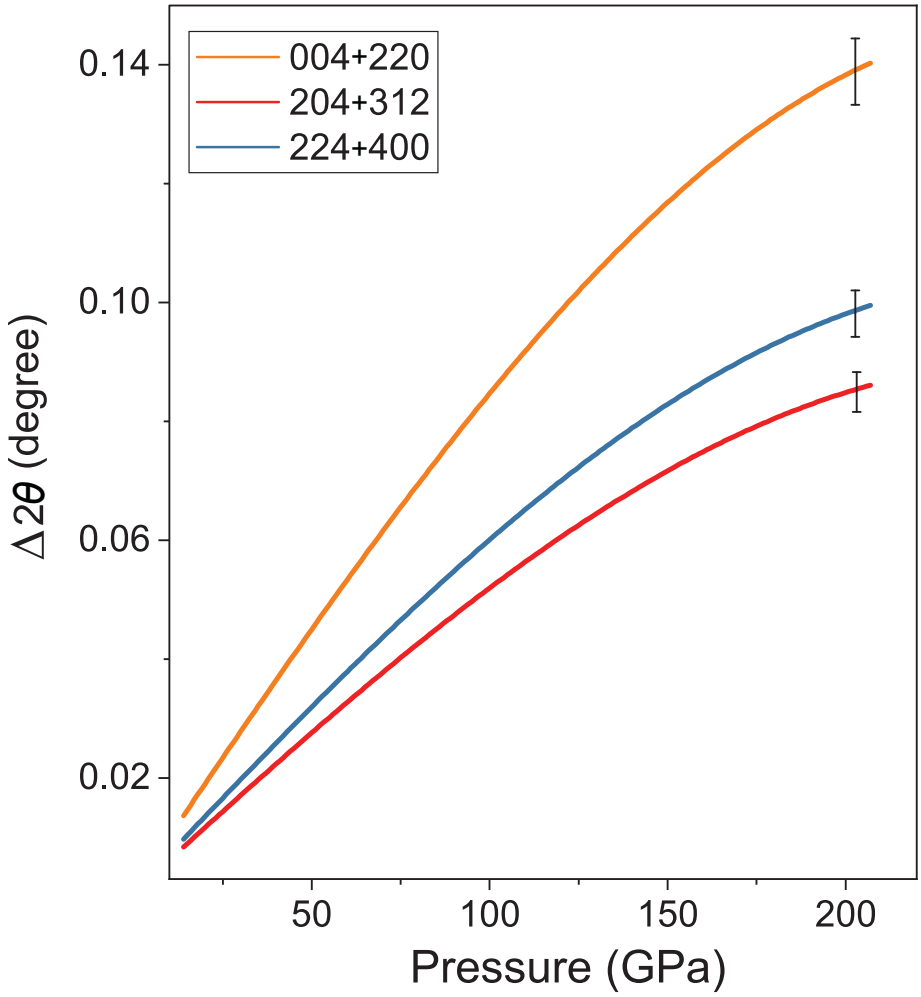

Figure 4

This is the peer-reviewed, final accepted version for American Mineralogist, published by the Mineralogical Society of America.
The published version is subject to change. Cite as Authors (Year) Title. American Mineralogist, in press.
DOI: https://doi.org/10.2138/am-2021-7913. http://www.minsocam.org/

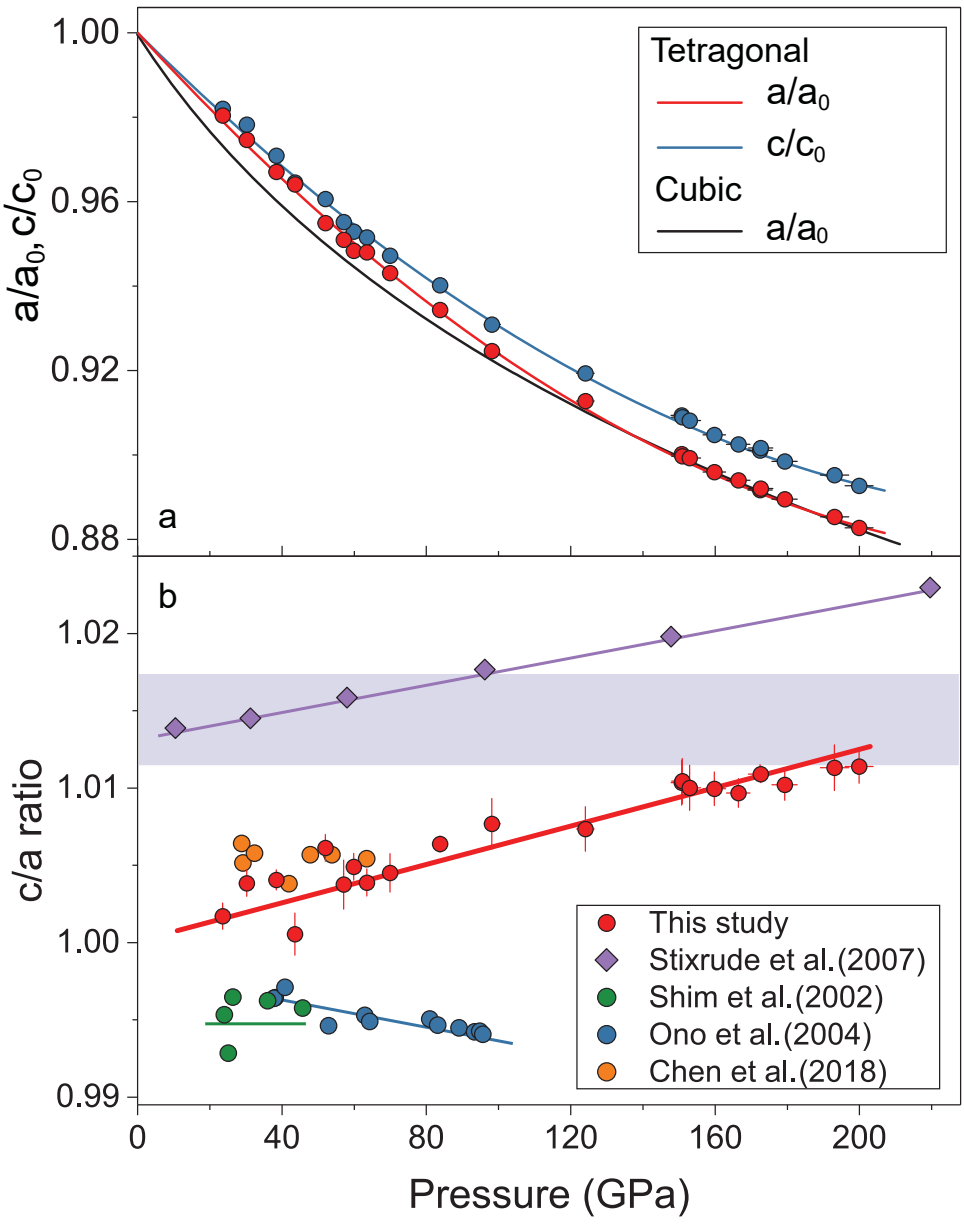

Figure 5

This is the peer-reviewed, final accepted version for American Mineralogist, published by the Mineralogical Society of America.
The published version is subject to change. Cite as Authors (Year) Title. American Mineralogist, in press.
DOI: https://doi.org/10.2138/am-2021-7913. http://www.minsocam.org/

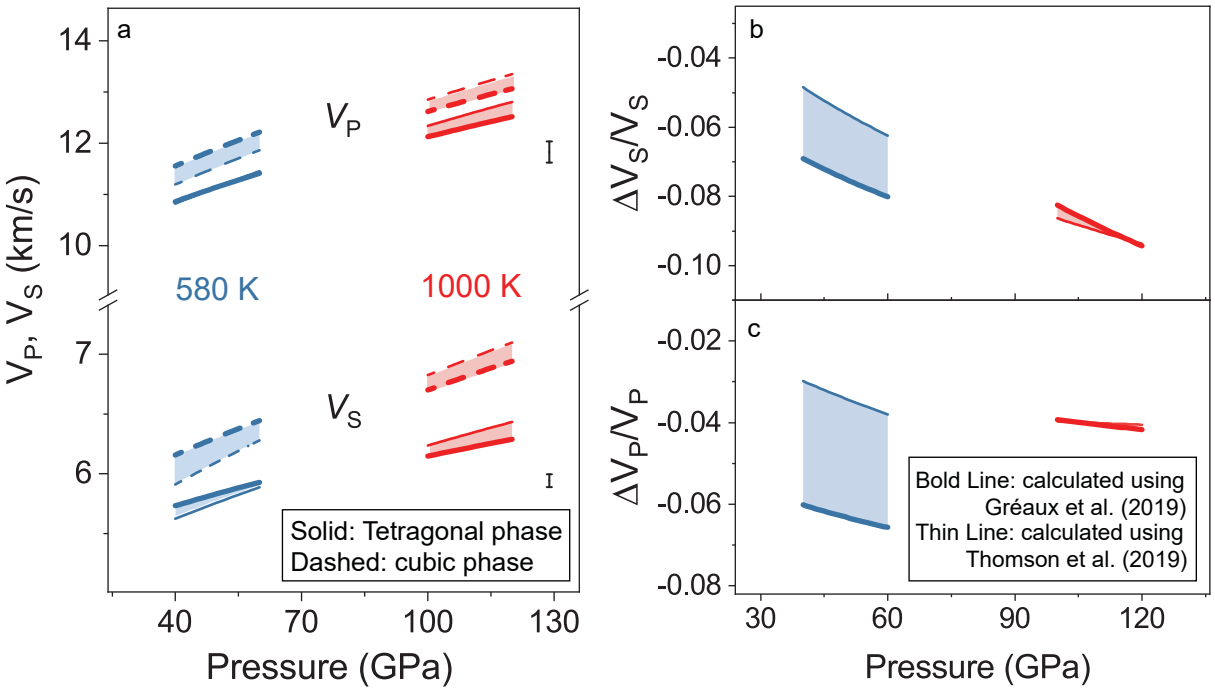

Figure 6